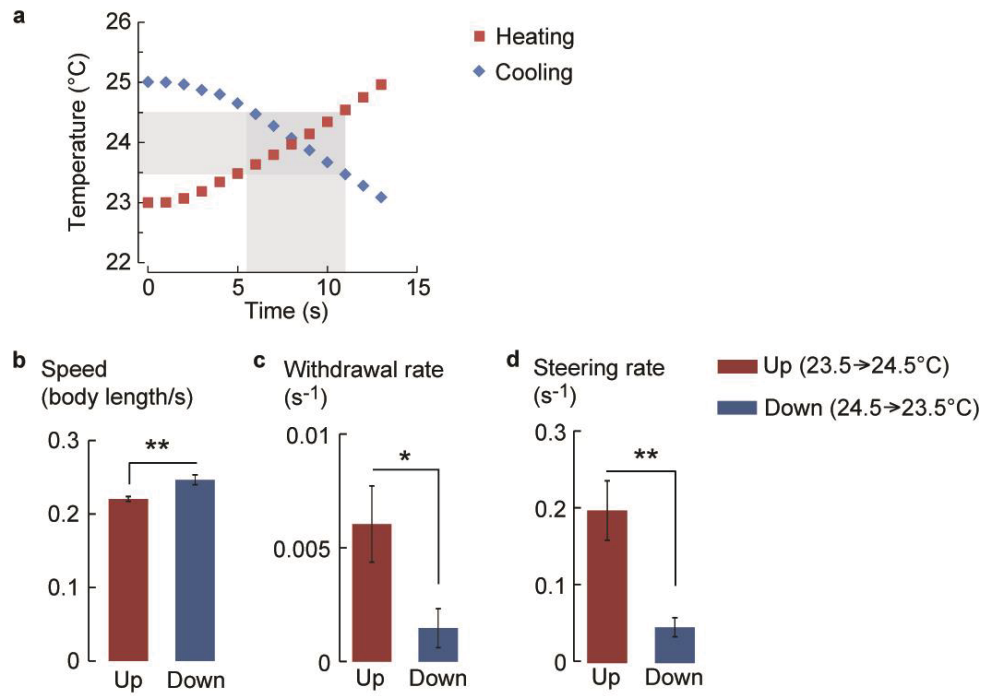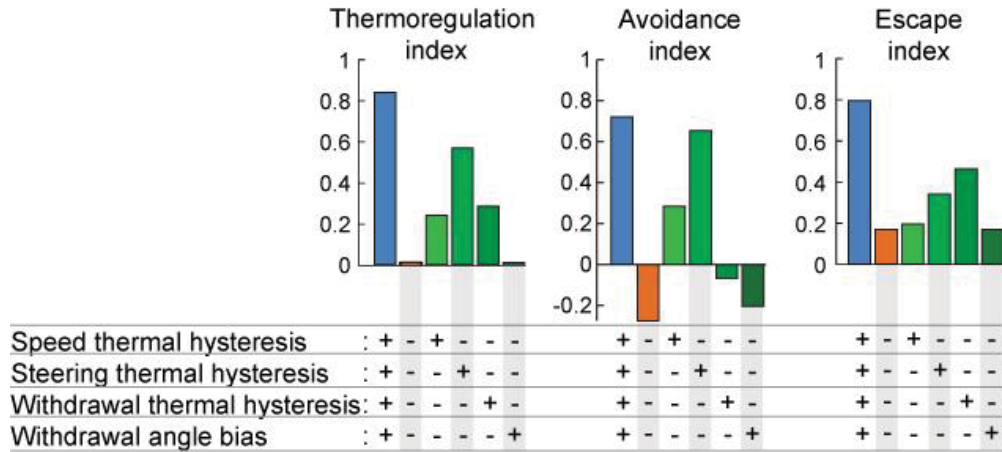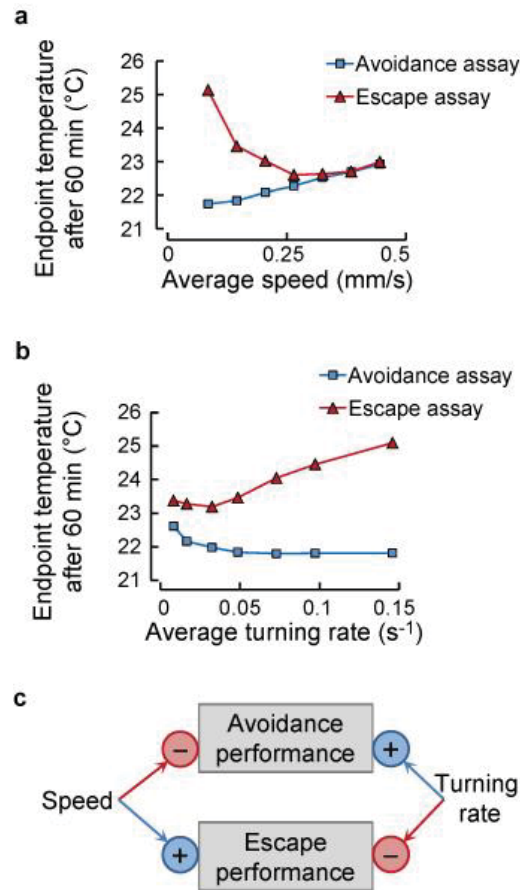**Supplementary Figure S1: Assay setup and thermal stimuli.** (**a**) Scheme showing the temporal thermal ramp assay setup. Worms crawling at the surface of the Petri dish were submitted to thermal rises or falls thanks to the depicted thermoelectric system. Two temperature probes (not depicted) were located at the surface of the aluminium plate and at the surface of the agar in the Petri dish, respectively. The first probe was used to feed back to a PID controller (not depicted) adjusting the current in the Peltier element for heating or cooling. The second probe was used to record temperature during experiments. Water flowing through a GPU cooling block was used to dissipate the heat generated by the Peltier element upon sample cooling. Oblique illumination was achieved with a square of 36 red LEDs. (**b**) Scheme showing the spatial thermogradient assay setup. The setup was similar to the temporal thermal ramp assay, except that two thermoelectric modules were connected by a rectangular aluminium plate to generate a linear temperature gradient. (**c**) Temperature time-course measured in the heating ($n=36$) and cooling ramp assays ($n=37$). The average thermal slopes determined over the linear portion of the curves are indicated. (**d**) Temperatures measured at the top of the agar surface along Petri dishes in spatial thermogradient assays, with indication of the average thermal slope ($n= 4$ measurements, with s.e.m. as error bars).
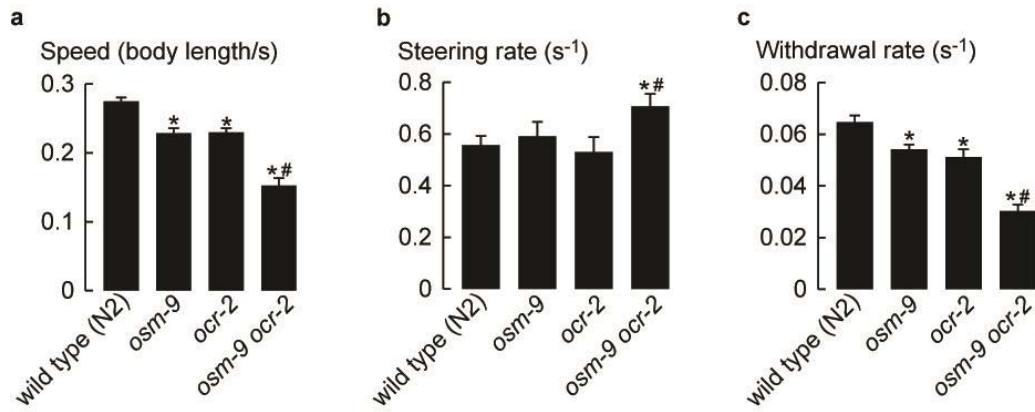
Supplementary Figure S2: Thermal stimuli lasting a few seconds are sufficient to cause thermal hysteresis for speed, steering, and withdrawal responses. Animals were equilibrated at 23 °C or 25 °C for 5 minutes and then were exposed to a sudden increase or decrease in temperature. (**a**) Thermal stimuli measured at the top of the agar surface, with indication of the specific window used for behavioural analyses between 23.5 and 24.5 °C (grey shade). (**b, c, d**) Comparison of behavioural data recorded during heating from 23.5 to 24.5 °C (up) and cooling from 24.5 to 23.5 °C (down). Results are means with s.e.m. as error bars (n=10 experiments with at least 15 worms each). **, P<.01; *, P<.05 by Student's t-tests.

Thermoregulation index Avoidance index Escape index

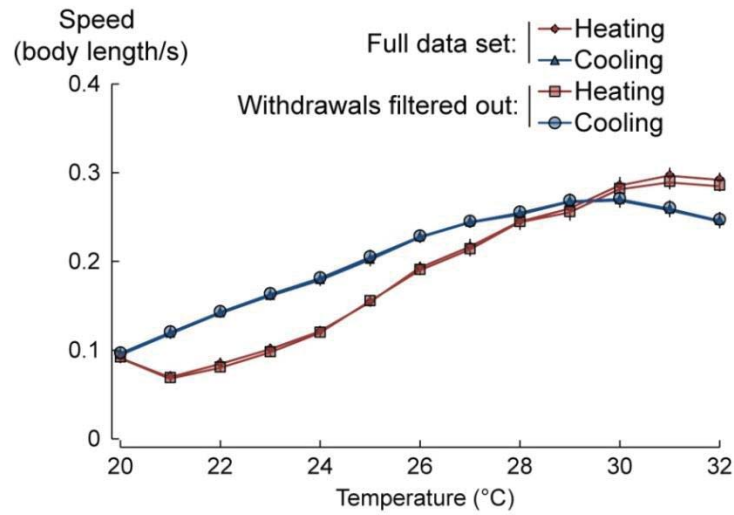|	Thermoregulation index						Avoidance index						Escape index					
Speed thermal hysteresis	+	-	+	-	-	-	+	-	+	-	-	-	+	-	+	-	-	-
Steering thermal hysteresis	+	-	-	+	-	-	+	-	-	+	-	-	+	-	-	+	-	-
Withdrawal thermal hysteresis	+	-	-	-	+	-	+	-	-	-	+	-	+	-	-	-	+	-
Withdrawal angle bias	+	-	-	-	-	+	+	-	-	-	-	+	+	-	-	-	-	+

Supplementary Figure S3: Computer simulations with single behavioural mechanisms. Simulations of worm long-range navigation in a linear gradient from 21°C to 35 °C (1.12 °C/cm). Starting temperatures were systematically varied to cover the innocuous-noxious range, from 22 to 32 °C. Worm performances were assessed with the Thermoregulation, Avoidance, and Escape indexes that were calculated from the median endpoint temperature reached by animals after 60 minutes (as in Figure 5). Depicted results compare a full model implementing the four identified behavioural mechanisms (Speed thermal hysteresis, Steering thermal hysteresis, Withdrawal thermal hysteresis, and Withdrawal angle bias), a model where all of them are inactivated, and four models with selective activation of each of the four behavioural mechanisms.
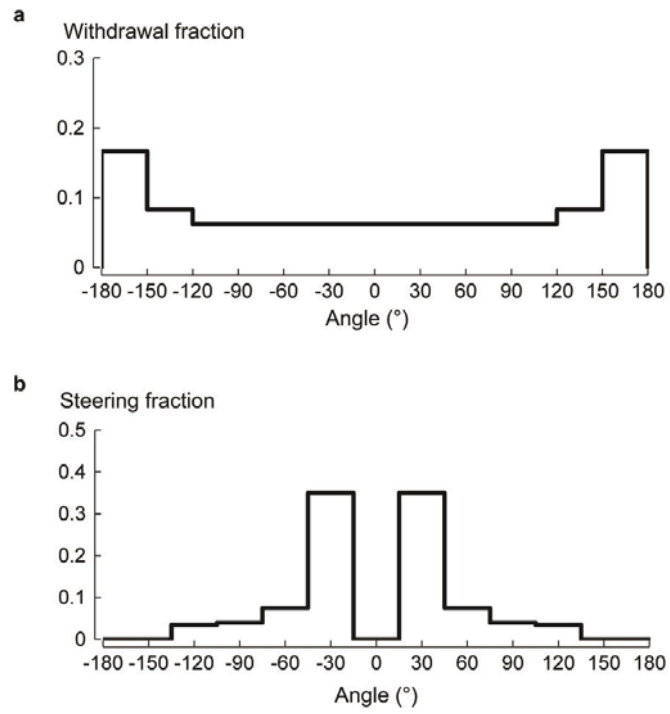
Supplementary Figure S4: Speed and turning rate have a counteracting effect on escape and avoidance. Worm navigation in thermogradients was simulated from a model integrating the full heat-exposure reduction mechanisms (as in Fig. 4). While maintaining the thermal hysteresis intact, the average speed and turning rate (both steering and withdrawal) were systematically modulated in a range arbitrarily defined around the data measured for wild-type worms. (**a**) Effect of speed variations. The median temperature reached by worms after 60 minutes was measured to assess worm performances in Avoidance and Escape assays (as in Fig. 4 b and c). (**b**) Effect of turning rate variations. The median temperature reached by worms after 60 minutes was measured to assess worm performances in Avoidance and Escape assays (as in Fig. 4 b and c). (**c**) Schematic of the conflicting impact of average speed and turning rate on the two complementary general strategies of avoidance and escape.
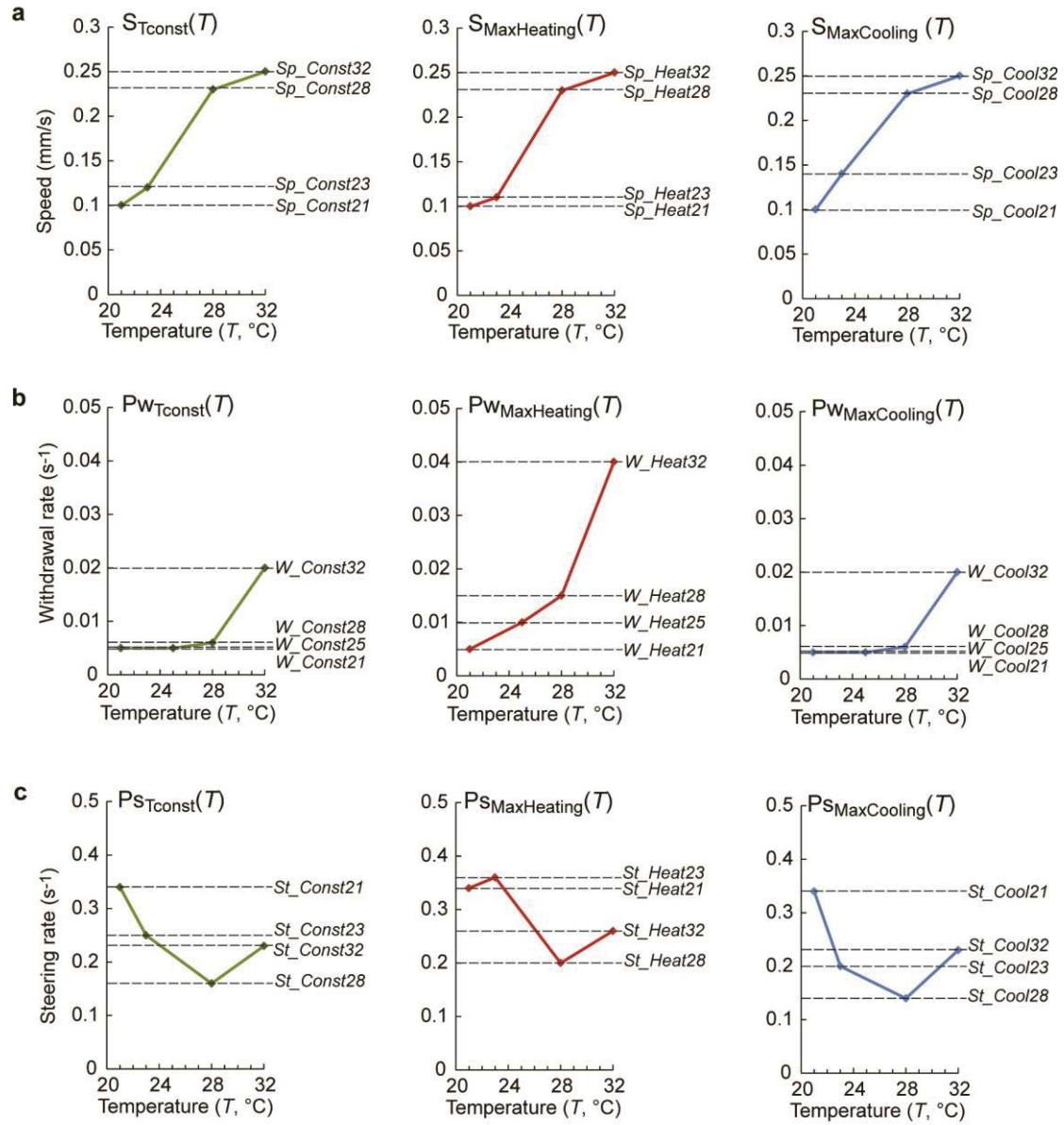
Supplementary Figure S5: *osm-9* and *ocr-2* act redundantly to control heat-evoked behaviours. Heat-evoked behaviours of wild-type (N2), *osm-9(ky10)*, *ocr-2(ak47)*, and the double mutant *osm-9(ky10) ocr-2(ak47)* were compared with heat ramp assays (as in Figure 7). (**a**) Speed at noxious temperatures was measured upon heating from 28 to 32 °C. (**b**) Steering rate was measured upon heating from 22 to 28 °C. (**c**) Withdrawal rate was measured upon heating from 29 to 32 °C. All results are expressed as mean, with s.e.m. as error bars (n≥10 experiments with at least 15 worms each). Separate one-way ANOVAs revealed a significant effect of the genotype for all three measures ($F_{(3,58)}$=13.22 to 50.11, $P<.001$). *, $P<.001$ versus wild-type (N2); #, $P<.001$ versus each single mutant calculated by Bonferroni *post-hoc* tests.

Supplementary Figure S6: Speed changes during withdrawals do not account for the speed thermal hysteresis effect. Movies of worm locomotion were recorded during heating and cooling temporal ramps as described in Figure 1. In order to evaluate the impact of withdrawals on the overall speed profiles, two analysis protocols to quantify speed were compared: first, a protocol including the full data set (as for the results depicted in Figure 1); second, a protocol filtering out the data points corresponding to withdrawals (from reversal to the end of the omega turn). Profiles obtained with the two approaches were almost superimposable. The small differences were not statistically different, as shown by two separate two-way ANOVAs (Filtering x Temperature) performed for heating and cooling, respectively (Heating, $F_{(25,390)} = 127.11$, Filtering effect: $P=.285$, Filtering x Temperature interaction effect: $P=1$; Cooling, $F_{(25,438)}= 65.35$, Filtering effect: $P=.584$, Filtering x Temperature interaction effect: $P=1$). These results indicate that the speed changes during withdrawals have a negligible impact on the overall speed profiles and do not account for the speed thermal hysteresis effect (described in Figure 1a).
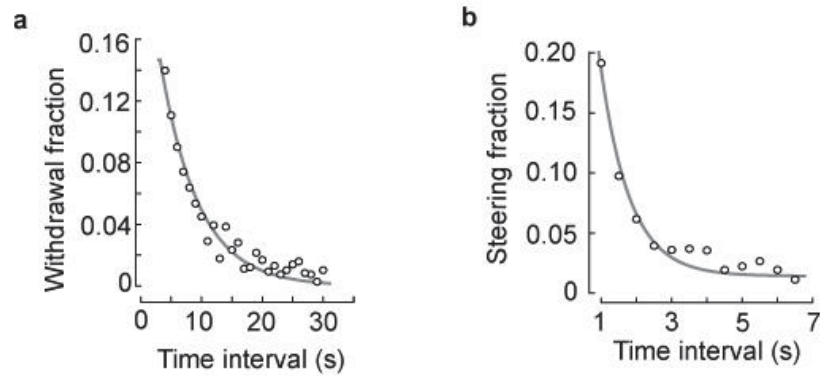
Supplementary Figure S7: Distributions of turn angles used in the behaviour simulations. (**a**) Distribution of turn angles taken upon withdrawal during simulations. (**b**) Distribution of turn angles taken upon steering during simulations.

Supplementary Figure S8: Parameter definition for behaviour simulations. (**a**) The speed of worms moving perpendicular to the gradient (S_{Tconst}), facing the hot side ($S_{MaxHeating}$), or facing the cool side of the gradient ($S_{MaxCooling}$) was expressed as a function of temperature; in each case with three affine functions for the 21-23, 23-28, and 28-32 °C intervals. The 12 input parameters for the simulations (*Sp_Const21*, *Sp_Const23*, *Sp_Const28*, *Sp_Const32*, *Sp_Heat21*, *Sp_Heat23*, *Sp_Heat28*, *Sp_Heat32*, *Sp_Cool21*, *Sp_Cool23*, *Sp_Cool28*, and *Sp_Cool32*) are depicted on the graphs. (**b**) The withdrawal probability of worms moving perpendicular to the gradient (Pw_{Tconst}), facing the hot side ($Pw_{MaxHeating}$), or facing the cool side of the gradient ($Pw_{MaxCooling}$) was expressed as a function of temperature; in each case with three affine functions for the 21-25, 25-28, and 28-32 °C intervals. The 12 input parameters for the simulations (*W_Const21*, *W_Const25*, *W_Const28*, *W_Const32*, *W_Heat21*, *W_Heat25*, *W_Heat28*, *W_Heat32*, *W_Cool21*, *W_Cool25*, *W_Cool28*, and *W_Cool32*) are depicted on the graphs. (**c**) The steering probability of worms moving perpendicular to the gradient (Ps_{Tconst}), facing the hot side ($Ps_{MaxHeating}$), or facing the cool side of the gradient ($Ps_{MaxCooling}$) was expressed as a function of temperature; in each case with three affine functions for the 21-23, 23-28, and 28-32 °C intervals. The 12 input parameters for the simulations (*St_Const21*, *St_Const23*, *St_Const28*, *St_Const32*, *St_Heat21*, *St_Heat23*, *St_Heat28*, *St_Heat32*, *St_Cool21*, *St_Cool23*, *St_Cool28*, and *St_Cool32*) are depicted on the graphs.

The parameter values for worms moving perpendicular to the gradient (S_{Tconst}, Pw_{Tconst}, and Ps_{Tconst}), and for which self-movement does not cause thermal changes, were derived from data recorded at constant temperatures. The parameter values for worms facing the hot side of the gradient ($S_{MaxHeating}$, $Pw_{MaxHeating}$, and $Ps_{MaxHeating}$) or facing the cool side ($S_{MaxCooling}$, $Pw_{MaxCooling}$, and $Ps_{MaxCooling}$) were derived from empirical data recorded in heating and cooling ramps by interpolating the parameter values from the calculated temporal thermal changes due to the animal self-movement. The values for the 36 input parameters are reported in Supplementary Data 1.

Supplementary Figure S9: Time interval distributions between successive withdrawals and steering events. (**a**) The time interval between successive withdrawal events was measured during heating ramps and their distribution was reported for 2 s bins. Data were fitted with a first order exponential with the formula $y = A * \exp(Bx)$ and the coefficients: A=.245; B=-.160. (**b**) The time interval between successive steering events was measured during heating ramps and their distribution was reported for 0.5 s bins. Data were fitted with a first order exponential with the formula $y = A * \exp(Bx)$ and the coefficients: A=.571; B=-1.202.

Supplementary Table S1: Selected behavioural parameters as a function of temperature

Temperature	Temperature change	Speed (body length/s) (mean ± s.e.m)	Steering rate (s^{-1}) (mean ± s.e.m)	Withdrawal rate (s^{-1}) (mean ± s.e.m)
22°C	Cooling ↓	0.142 ± 0.006 *c*	0.14 ± 0.03 *b,c*	0.004 ± 0.002 *c*
	Constant →	0.124 ± 0.004 *c*	0.35 ± 0.05 *a,c*	0.006 ± 0.001 *c*
	Heating ↑	0.085 ± 0.006 *a,b*	0.70 ± 0.05 *a,b*	0.027 ± 0.005 *a,b*
25°C	Cooling ↓	0.203 ± 0.008 *c*	0.06 ± 0.02 *c*	0.002 ± 0.001 *c*
	Constant →	0.186 ± 0.007	0.24 ± 0.03 *c*	0.005 ± 0.001 *c*
	Heating ↑	0.155 ± 0.006 *a*	0.59 ± 0.07 *a,b*	0.038 ± 0.004 *a,b*
28°C	Cooling ↓	0.254 ± 0.007	0.05 ± 0.02 *c*	0.003 ± 0.001 *c*
	Constant →	0.223 ± 0.008	0.16 ± 0.02 *c*	0.006 ± 0.001 *c*
	Heating ↑	0.246 ± 0.009	0.33 ± 0.02 *a,b*	0.038 ± 0.006 *a,b*
32°C	Cooling ↓	0.246 ± 0.009 *c*	0.26 ± 0.03 *c*	0.023 ± 0.002 *c*
	Constant →	0.250 ± 0.008	0.23 ± 0.03 *c*	0.019 ± 0.003 *c*
	Heating ↑	0.293 ± 0.007 *a*	0.53 ± 0.03 *a,b*	0.076 ± 0.006 *a,b*

Differences were assessed with two-way ANOVAs followed by Bonferroni *post-hoc* tests: *a*, $P<.01$ versus Cooling; *b*, $P<.01$ versus Constant; *c*, $P<.01$ versus Heating.

Supplementary Note 1

In the present research, we studied worms that had been starved for 5 to 8 hours, a protocol developed in a previous study[24]. This treatment has two advantages. First, it suppresses the thermotaxis response of animals[1], which allows removing one layer of behavioural complexity and focusing on avoidance/escape behaviours, regardless of any learned thermal preference. Second, because worms are tested off-food, we get rid of the acute food removal effects, which in worms have a profound impact on navigation behaviors[33]; after several hours of starvation, animal behaviour is more stable. The main limitation of using this starvation protocol is that our conclusions are restricted to starved animals. However, using the simpler starved animal model was a reasonable and useful starting approach to disentangle the relatively complex behavioural mechanisms implicated in escape and avoidance. Additional research is required to address how these mechanisms are affected by food availability and how they integrate with thermotaxis mechanisms.

Our genetic analysis revealed that signalling through TRPV and NPR-1 plays a role in controlling noxious heat escape and avoidance. Animals with non-functional TRPV signalling through OSM-9 and OCR-2 channels have decreased speed thermal hysteresis, dampened speed dynamic tuning range, increased steering rate, but decreased heat-induced withdrawal rate (Fig. 7). All these effects converge to make them poor escapers, but they retain relatively good avoidance abilities. Conversely, animals with non-functional signalling through the NPR-1 receptor have increased baseline speed, decreased steering rate, and decreased withdrawal rate at intermediate temperatures (Fig. 7). All these effects converge to make them poor avoiders, but they remain relatively good escapers. The fact that both TRPV mutants ("blocked" in the avoidance regime) and NPR-1 mutants ("blocked" in the escape regime) have impaired thermoregulatory performances highlights the importance of dynamic transitions between avoidance and escape regimes. It is not clear how mutations affecting TRPV and NPR-1 signalling cause these changes. OSM-9 and OCR-2 channels might be thermosensors, as are their mammalian orthologs[39,40], albeit there is no direct evidence that they form heat-gated channels in

worms. As an alternative mode of action, TRPV channels might work in thermosensory neurons to amplify or integrate transduced signals, as suggested for mechano-nociception in the ASH neuron[7]. TRPV channels might also act more indirectly, e.g. by modulating neuroendocrine secretion[41]. Regarding NPR-1, it seems very unlikely that it functions as a thermosensor. Actually, the main effects caused by the *npr-1* mutation are unrelated to the heat stimulation (increased speed and decreased steering rate below 25 °C). Thus, it is possible that *npr-1* mutation works solely by making worms hyperactive at low temperatures, regardless of any heat detection mechanism. Nevertheless, the *npr-1* mutation still alters worm performances in avoidance assays. This result highlights the importance of considering "baseline behaviour" and its modulation when studying how a given stimulus impacts navigational behaviours. Additional studies will be required to clarify how TRPV and NPR-1 signalling affect worm navigation behaviour in thermogradients.

Supplementary Methods:

Movie analyses and behavioural event flagging

Movies were analysed off-line with the Multi-Worm Tracker software[23]. For each frame, the software identifies objects (animals) and records the coordinates of their centres of mass, the coordinates of an eleven point skeleton matching each animal, as well as animal *Length* (linearly measured from one object extremity to the other) and *Width* (linearly measured perpendicularly to the *Length* axis). Objects were tracked over the full movies. We used custom designed spreadsheets to compute raw data and extract the relevant behavioural parameters. All data were smoothed on a five frame interval (centred moving average of the centre of mass coordinates, as well as of the skeleton coordinates). Tracks terminated when worms moved out of the field or upon worm collision. To remove potential artefacts caused by these events and by the data smoothing with moving averages, we removed the data corresponding to the first ten and last ten frames of each track.

Speed- To compute instant *Speed*, we compared the position of the centre of mass between successive frames. To minimize the impact of potential variations in animal size across experiments or genotypes, *Speed* values for each track were divided by the average animal *Length* measured over the full track, such that we report speed in body length per second. Of note, we observed identical results without this normalization step (data not shown), suggesting that variations in animal size were not significant, at least for the particular set of strains tested here. The speed measures reported in the Result section include all data points, without filtering out measures taken during particular behavioural events. To rule out the possibility that the speed thermal hysteresis effect reported here (Fig. 1a) was due to animals moving slower during heat-induced omega turns, we performed control analyses that excluded data during withdrawal events. Speed profiles with and without this filtering were undistinguishable (Supplementary Fig. S6), indicating that the speed modulation during withdrawals had no significant impact.

Steering- In order to detect Steering events, the *Direction of movement* of each object was compared between successive frames. The *Direction of movement* was calculated by comparing an object's centre of mass coordinates between a given frame and the previous frame. The *Angle change* was computed by comparing the *Direction of movement* between a given frame and the previous frame. Frames were flagged for a Steering event if the *Angle change* was between 15° and 135° or between -15° and -135°. Consecutive frames flagged as Steering events were counted as separate events.

Withdrawal- A withdrawal was defined as a succession of Reversal and Omega turn events. Frames were flagged for Reversal if the *Angle change* was between 150° and 180° or between -150° and -180°. The definition of Omega turn was based on the *Head to tail distance* (distance between the two terminal ends of the skeleton) and the object *Length*/*Width* ratio. Two criteria needed to be fulfilled for a frame *n* to be flagged as Omega. First, a drop of more than 20% between the *Head to tail distance* averaged on frames *n-2* to *n-5* and the *Head to tail distance* averaged on frames *n+2* to *n+5*. Second, at least one frame between frame *n-5* and *n+5* for which the *Length*/*Width* ratio was below 2.

Criteria definition, artefact filtering, and method validation- All the criteria presented here-above have been set empirically by analysing a sample set of ten long tracks showing several occurrences of the event of interest during an heating ramp. We tuned the criteria cut-offs and the size of the data smoothing windows to ensure flagging all the relevant events visually identified, while not picking artefacts. We also focused on the sections where worms get paralyzed (at temperature above 36 °C, data not shown), in order to evaluate the intrinsic noise due to imaging and tracking. We found that very slow moving, pausing, or paralyzed worms were producing many artefacts (especially for Reversal and Steering), which were not satisfactorily handled by tuning the cut-offs. Thus, we filtered out any flagged Reversal and Steering events for which *Speed* was not above 0.013 body length/s in at least one of the five encompassing frames. To validate our criteria for reversal and omega turns, we compared 25 tracks from five heating ramp movies taken on five different days. Visual and computer-detection were matching for 139 omega turns and 85 reversals. Computer-detection yielded 4 false negatives and 9 false positives for omega turns; and 8 false negatives and 4 false positives for reversals. Thus the sensitivity and the specificity of our computer detection are above 90%. For gradient experiments,

14

where the field of view was larger and animals appeared smaller, results were not as satisfactory and withdrawal events were flagged manually. Worms sometimes curve steeply when exiting omega turns, which might have led to Steering event false positives. Because worm speed is low during omega turns, most of such artefacts were removed by the speed threshold (see above). The fraction of the remaining Steering events that were concomitant to omega turns or flagged during the two subsequent frames was negligible (1.6 %).

Computer simulation of behaviour

Simulation unfolding- Worm locomotion in linear thermogradients was simulated using custom written spreadsheets and Visual Basic macros. For each simulation, 500 animals were run sequentially. Animals were considered as punctual objects evolving in a 12.5 cm long (x axis) and 7 cm large (y axis) dish, with a linear thermogradient from 21 to 35 °C along the x axis. Animals started at defined positions in the gradient: x coordinate was manipulated to match the desired starting temperature, while y coordinate was randomized. Their initial direction was random. Animals reaching the dish border were set to restart locomotion perpendicularly to the border. Animal coordinates were refreshed at intervals of one second and monitored over 60 minutes.

For every time interval, animals did three things:

1) they moved according to their precedent direction for a distance defined by their speed (a new position was then defined)
2) they decided whether to do a withdrawal
3) they decided whether to do a steering event

Each time a withdrawal occurred, the animal position was frozen for five seconds and then animal restarted locomotion in a new direction calculated from the implemented withdrawal angle distribution (Supplementary Fig. S7a). Each time a steering event occurred, the animal direction was changed according to the implemented steering angle distribution (Supplementary Fig. S7b). If neither withdrawal nor steering happened, animal continued in the same direction.

Speed calculation- At every position, the speed magnitude was calculated as a function of temperature (T) and corrected for thermal hysteresis effects by taking into account the angle, θ, formed between the current worm direction and the direction producing maximal heating (due to self-movement). The instant animal speed S(T, θ) was set for animals moving *up* or *down* the gradient as follows:

$$S_{down}(T, \theta) = S_{Tconst}(T) + \cos(\theta)^* (S_{MaxCooling}(T) - S_{Tconst}(T))$$

$$S_{up}(T, \theta) = S_{Tconst}(T) + \cos(\theta)^* (S_{MaxHeating}(T) - S_{Tconst}(T))$$

The first term, $S_{Tconst}(T)$, accounts for the simple effect of temperature and was based on empirical measures of animal speed at constant temperatures (see parameter definition in Supplementary Fig. S8 and their values in Supplementary Data 1). The second term, $\cos(\theta)^* (S_{MaxCooling/Heating}(T) - S_{Tconst}(T))$, accounts for the thermal hysteresis correction. ($S_{MaxCooling}(T) - S_{Tconst}(T)$) and ($S_{MaxHeating}(T) - S_{Tconst}(T)$) represent the maximal corrections when animals face the cool or the hot side of the gradient, respectively. The model assumes that the speed thermal hysteresis effect is proportional to the slope of the thermal change and this is why the thermal hysteresis correction term is proportional to $\cos(\theta)$. When animals face the cool or the hot side of the gradient, the amplitude of the thermal changes induced by self-movement is maximal ($\cos(\theta)=1$ or -1). When animals run perpendicular to the gradient, self-movement induces no thermal change and the thermal hysteresis correction term is null ($\cos(\theta)=0$). $S_{MaxCooling}(T)$ and $S_{MaxHeating}(T)$ functions were derived from empirically determined parameters (see parameter definition in Supplementary Fig. S8 and their values in Supplementary Data 1).

Withdrawal and steering probability calculation- To implement steering and withdrawal behaviours, we followed the same rationale and assumptions as for speed (see above). At every position, the probability of steering Ps(T, θ) and the probability of withdrawal Pw(T, θ) were set for animals moving *up* or *dow*n the gradient as follows:

$$Ps_{down}(T, \theta) = Ps_{Tconst}(T) + \cos(\theta)^* (Ps_{MaxCooling}(T) - Ps_{Tconst}(T))$$

$$Ps_{up}(T, \theta) = Ps_{Tconst}(T) + \cos(\theta)^* (Ps_{MaxHeating}(T) - Ps_{Tconst}(T))$$

$$Pw_{down}(T, \theta) = Pw_{Tconst}(T) + \cos(\theta)^* (Pw_{MaxCooling}(T) - Pw_{Tconst}(T))$$

$$\text{Pw}_{up}\ (T,\ \theta) = \text{Pw}_{\text{Tconst}}\ (T) + \cos(\theta)^* \ (\text{Pw}_{\text{MaxHeating}}\ (T) - \text{Pw}_{\text{Tconst}}\ (T))$$

The first term, $\text{Ps/w}_{\text{Tconst}}\ (T)$ accounts for the simple temperature dependency of these behaviours and is based on data recorded at constant temperatures. The second terms are the thermal hysteresis corrections, which, like for speed, depend on θ and on empirical data-derived parameters for $\text{Ps}_{\text{MaxCooling}}$ (T), $\text{Ps}_{\text{MaxHeating}}\ (T)$, $\text{Pw}_{\text{MaxCooling}}\ (T)$, and $\text{Pw}_{\text{MaxHeating}}\ (T)$ (see parameter definition in Supplementary Fig. S8 and their values in Supplementary Data 1).

The choice of a probabilistic model for the implementation of steering and withdrawal behaviours was based on empirical data. Indeed, the distribution of the time intervals between consecutive withdrawal events measured during heating ramps was fitted by a single exponential decay function, suggesting that heat-evoked withdrawals occur independently of each other, in a stochastic manner (Supplementary Fig. S9a). Similar observations were made for steering events (Supplementary Fig. S9b).

Behavioural mechanism manipulation- To artificially disable behavioural mechanisms (Fig. 5), the model was modified as follow:

- Speed thermal hysteresis off: the speed-temperature profiles for heating and cooling were matched to the one for constant temperature.
- Steering thermal hysteresis off: the steering rate-temperature profiles for heating and cooling were matched to the one for constant temperature.
- Withdrawal thermal hysteresis off: withdrawal rate-temperature profile for heating and cooling were matched to the one for constant temperature.
- Withdrawal angle bias off: turn angles caused by withdrawals were random (instead of being taken from the distribution in Supplementary Fig. S7a).

To artificially disable the dynamic tuning (Fig. 6), the model was modified by removing the temperature effects on speed, steering rate and/or withdrawal rate. Values for heating, cooling, and constant temperature, respectively, were set as their average over the 21-35 °C range, such that the overall thermal hysteresis was maintained.

Supplementary References

39.   Tominaga M, Caterina MJ, Malmberg AB, Rosen TA, Gilbert H, Skinner K*, et al.* The cloned capsaicin receptor integrates multiple pain-producing stimuli. *Neuron* 1998, **21**(3)**:** 531-543.

40.   McKemy DD. Temperature sensing across species. *Pflugers Arch* 2007, **454**(5)**:** 777-791.

41.   Lee BH, Ashrafi K. A TRPV channel modulates C. elegans neurosecretion, larval starvation survival, and adult lifespan. *PLoS Genet* 2008, **4**(10)**:** e1000213.